

Rhombic-magnetoelastic/metal-organic framework functionalized resonators for highly sensitive toluene detection.

Paula G. Saiz^{*1,2}, Roberto Fernandez de Luis¹, Luis Bartolome³, Jon Gutiérrez^{1,4},

María Isabel Arriortua^{1,2}, Ana Catarina Lopes^{1,5,6}

¹BCMaterials, Basque Center for Materials, Applications and Nanostructures, UPV/EHU Science Park, 48940 Leioa, Spain

²Dept. of Mineralogy and Petrology, Science and Technology Faculty, University of the Basque Country (UPV/EHU), Barrio Sarriena s/n, 48940, Leioa, Spain

³Advances Research Facilities (SGIker), University of the Basque Country (UPV/EHU), Barrio Sarriena s/n, 48940, Leioa, Spain

⁴Dept. of Electricity and Electronics, Science and Technology Faculty, University of the Basque Country (UPV/EHU), Barrio Sarriena s/n, 48940, Leioa, Spain

⁵Centre for Cooperative Research on Alternative Energies (CIC energiGUNE), Basque Research and Technology Alliance (BRTA), Alava Technology Park, Albert Einstein 48, 01510 Vitoria-Gasteiz, Spain.

⁶IKERBASQUE, Basque Foundation for Science, Plaza Euskadi 5, 48009 Bilbao, Spain

*Corresponding author: saizpg@gmail.com

Table of Contents

1. Materials and Processing Methods	2
1.1. Chemicals.....	2
1.2. Synthesis of UiO-66-NH ₂	2
1.3. Spray coating technique.....	2
2. Characterization Techniques and Procedures	3
2.1. Powder X-ray diffraction.....	3
2.2. Fourier-transform infrared spectroscopy.....	3
2.3. Thermogravimetric analysis.....	3
2.4. N ₂ adsorption isotherms.....	4
2.5. Scanning and Transmission Electron Microscopies.....	4
3. Performance Assessment	5
3.1. Magnetoelastic characterization.....	5
3.2. Theoretical resonance frequency for rhombic resonators.....	5
3.3. Multiple Headspace solid-phase microextraction.....	6
3.4. Toluene sensing experiments.....	7
4. Supplementary Figures	8
5. Supplementary Tables	14

1. Materials and Processing Methods

1.1. Chemicals

All chemicals and solvents used were obtained commercially. Zirconium(IV) chloride (99.5%, Alfa Aesar), 2-aminoterephthalic acid (BDC-NH₂) (99%, Sigma Aldrich), N,N-dimethylformamide (DMF) (99.8%, Sigma Aldrich), liquid toluene (99.8%, Sigma Aldrich) and Nitrogen gas (Alphagaz Nitrogen, Air Liquide) have been used. All the chemicals were used without further purification.

1.2. Synthesis of UiO-66-NH₂

UiO-66-NH₂ MOF was prepared through a slightly modified solvothermal synthesis [1,2]. First, 0.5418 g of zirconium chloride were dissolved in 60 mL of DMF under magnetic stirring in a Pyrex[®] autoclave. Afterwards, 0.4185 g of BDC-NH₂ and 1.5 mL of distilled water were added to the zirconium chloride solution under continuous stirring at room temperature. Once a clear solution was obtained, the Pyrex[®] reactor was closed and placed in a preheated oven at 80°C during 24 hours. After that, the sample was allowed to cool down to room temperature and the obtained yellow powder was recovered by centrifugation and washed three times overnight with methanol. The solvent exchange process was repeated three times in order to remove the unreacted ligand and exchange the residual DMF present at the pores. Finally, the compound was dried at 80°C during 12 hours. A schematic diagram of the MOF synthesis process is shown in Figure S1.

1.3. Spray coating technique

The powder MOF was deposited onto the surface of the magnetoelastic resonator by the spraying technique. An Iwata eclipse HP-SBS airbrush was used for that. The different deposition parameters were optimized in order to obtain the best layer properties. In particular, different solvents (i.e. acetone, ethanol, isopropanol...) were used to prepare the MOF suspensions. Among them, isopropanol results the best option since it lead to a more homogeneous layer which is probably related with its evaporation rate. A good dispersion of the MOF was found when using ultrasonication. Moreover, the operation temperature was also adjusted in order to improve the layer properties. Initially the spray depositions were performed at room temperature but it was observed that the deposited layer was not homogeneous and present lot microcracks probably related with the slow evaporation process. Afterwards,

spraying was carried out by heating the tape at different temperatures in a heating plate and it was observed that the surface became much more homogeneous with increasing temperature because the solvent evaporates more quickly. After different tests, we conclude that a temperature of 120 °C is an optimal temperature to obtain a homogeneous layer. By controlling all these properties as well as the distance and the pressure homogeneous layers with controllable thickness are obtained. Thus, UiO66-NH₂ based ink with a concentration of 10 mg/mL was prepared dispersing 100 mg of the dried MOF powders on 10 mL isopropanol solution by ultrasonication during 20 min. The UiO66-NH₂ dispersion was sprayed onto the rough surface of the Metglas ribbon heated at 120°C. The mass gain after the spray deposition was thoroughly controlled. SEMOF-1 (74 µg of UiO66-NH₂ active layer) and SEMOF-2 (130 µg of UiO66-NH₂ active layer) samples were prepared by additive spraying methodology. A scheme of the spray functionalization process as well as microscope images of the resonator before and after the functionalization process are shown in Figure S2.

2. Characterization Techniques and Procedures

2.1. Powder X-ray diffraction

The powder X-ray diffraction (PXRD) patterns of the UiO66-NH₂ powder MOF, the bare Metglas resonator and the UiO66-NH₂/Metglas fabricated sensor were obtained at room temperature with a Panalytical X'pert CuK α diffractometer in the following conditions: 2 θ range = 5–70°, step size = 0.05°, exposure time = 10 s per step. Panalytical X'pert is a polycrystalline sample diffractometer with theta-theta geometry, a programmable slit, secondary graphite monochromator adjusted to a copper radiation and fast solid state PixCel detector adjusted to a 3.347° active length in 2 θ (°). The equipment allows to perform high quality measurements for the subsequent data processing. Full peak fit profile matching of the UiO66-NH₂ MOF was performed and results are shown in Figure S3.

2.2. Fourier-transform infrared spectroscopy

Fourier-transform infrared spectroscopy (FTIR) spectra measurements were carried out using a Jasco FT/IR-6100 spectrometer in Attenuated Total Reflectance mode (FTIR-ATR). Each spectrum was recorded from 600 to 4000 cm⁻¹ with a 1 cm⁻¹ resolution. 64 scans were measured and averaged to obtain the final spectra.

2.3. Thermogravimetric analysis

Thermogravimetric analysis (TGA) was performed under synthetic air (25 mL/min) with a NETZSCH STA 449F3 DSC–TGA thermo-balance instrument. This equipment allows adjusting the heating rate, controlling the measurement atmosphere and selecting the temperature program. An alumina crucible containing ca. 25 mg of the sample was heated at 5 °C min⁻¹ in the temperature range 30–700 °C.

Thermogravimetric analysis was performed in order to quantify the defect degree within the UiO66-NH₂ MOF structure. The linker-defect positions average per formula was estimated from the weight loss associated to the organic linker calcination step (at an approximately temperature of 300°C) [3,4] observed in the TGA curve (Figure S4). Assuming that the complete dehydration of the zirconium hexanuclear clusters occurs before the organic linker calcination step, the theoretical weight loss associated to the linker release as function of the defect degree can be calculated (Table S1) based on the following equation:



where x is the defect degree. The theoretically calculated data can be fitted to a linear equation (Figure S5) that has been used to determine the experimental defects per formula from the experimental weight loss obtained from the thermogravimetric curves (Figure S4).

2.4. N₂ adsorption isotherms

N₂ sorption isotherms were obtained at 77 K with a Quantachrome Autosorb iQ instrument. Approximately 30 mg of the samples were degassed at 120°C in high vacuum for at least 8 h prior to the measurement. The surface area value was obtained by the fitting of the adsorption data to a linearized form of the Brunauer–Emmett–Teller (BET) equation [5]. Results are shown in Figure 4c, Figure S6 and Table S2.

2.5. Scanning and Transmission Electron Microscopies

The morphology of the UiO66-NH₂ MOF nanoparticles was observed by Transmission Electron Microscopy (TEM) using a Philips Supertwin CM200 transmission microscope operated at 200 kV and equipped with a LaB6 filament and EDAX-DX-4 microanalysis system. The equipment incorporates double tilting sample holder, a Megaview III rapid acquisition camera, and a high resolution (4K x 4K) and high sensitivity digital camera. TEM images of the powder UiO66-NH₂ MOF are shown in Figure S7.

Moreover, the resonator functionalization was analyzed by using a Scanning Electron Microscopy (SEM) (JEOL JSM-7000F) operating at 10 kV. Prior to analysis, samples were coated with a gold layer of 15 nm using the Quorum Q150TS turbo pumped coater.

3. Performance Assessment

3.1. Magnetoelastic characterization

The magnetoelastic resonance behaviour of the resonators was characterized with a home-mounted magnetoelastic resonance detection system. The system consists on 2 coaxial solenoids, where the external solenoid generates a DC magnetic field (or bias) for modulation of the signal through an HP 6653A DC power supply and the inner solenoid (primary coil) which applies an AC magnetic field of small amplitude which drives the sample to the resonance. Then, the induced signal in the sample is measured through an air compensated pick-up coil (secondary coil) placed within the two coaxial solenoids, and is then monitored in an HP3589A Spectrum Analyzer. This spectrum analyser allows (i) to provide the AC voltage to excite magnetically the resonator via the primary coil and (ii) to observe the induced signal in a wide frequency range, including the magnetoelastic resonance one. The whole process is fully automatized and data is recorded in the computer. Two programs in the computer are assigned to the measurements system, the first one to measure the resonance frequency as a function of the applied DC magnetic field, and the second one to measure the resonance frequency as function of the time at a fixed DC magnetic field (usually the corresponding one to the maximum resonance amplitude). A scheme of the experimental set-up is shown in Figure S8, while the measured magnetoelastic resonance frequency as a function of the applied DC magnetic field can be seen in Figure S9.

3.2. Theoretical resonance frequency for rhombic resonators

The theoretical resonance frequency of a freestanding rhombus shaped magnetoelastic resonator of length L and in the first resonance mode ($n=1$), is given by [6]:

$$f_r^{rh} = \sqrt{\frac{\pi^2 + 4}{\pi^2 - 4}} \cdot \left(\frac{1}{2L} \cdot \sqrt{\frac{E}{\rho(1 - \nu^2)}} \right) \quad (S2)$$

where E is the Young modulus, ρ is the density and ν is the Poisson coefficient of the sensing material. Considering the elastic parameters of the Metglas sample (Density (ρ) of 7900 kg/m³ and Poisson's ratio (ν) of 0.33) and the rhombic sensor length (10 mm), the consequent

theoretical resonance frequency for a Young modulus (E) of 135 Gpa is calculated to be 335 kHz.

3.3. Multiple Headspace solid-phase microextraction

The ability of the samples to adsorb toluene was firstly assessed in static conditions by means of Headspace solid-phase microextraction (Figure S10). For that, an Agilent HP 6890 Gas Chromatograph coupled to an Agilent HP5973 Mass Spectrometer with a COMBI PAL injector (CTC Analytics) was used. A desorption temperature of 150°C was employed. Before the experiment, the samples were exposed to a toluene rich atmosphere during 60 minutes.

In addition, an estimation of the toluene adsorption capacity of the powder UiO66-NH₂ MOF was obtained by means of Multiple Headspace Solid-Phase Microextraction (MHS-SPME). In this method, it is considered that the sum of infinite successive extractions gives the total area of the adsorbed analyte, and hence, an estimation of the analyte mass present in the sample [7]. This can be reduced to a finite number of extractions having that the total analyte area (A_T) is given by equation S3 [8]:

$$A_T = \sum_{i=1}^{\infty} A_i = \frac{A_1}{1 - \beta} \quad (\text{S3})$$

where i is the extraction number, A_1 is the area of the first extraction peak and β is a constant. This constant is obtained by representing the logarithm of the i -th extraction area ($\ln A_i$) as function of the $(i-1)$ value, having that:

$$\ln A_i = \ln A_1 + (i - 1) \cdot \ln \beta \quad (\text{S4})$$

Thus, the β factor is obtained from the slope ($\ln \beta$) of the linear adjustment and from that the total area (A_T) is estimated from β allowing to obtain the analyte mass adsorbed in the sample ($m_{analyte}$) by using a calibration reference taking into account that:

$$m_{analyte} = \frac{\sum A_{T \text{ analyte}}}{\sum A_{T \text{ reference}}} \cdot m_{reference} \quad (\text{S5})$$

where $m_{reference}$ is the known reference mass, $A_{T reference}$ is the total area estimated for the calibration reference sample and $A_{T analyte}$ is the total area estimated for the analyte sample.

Thus, successive desorption cycles in the UiO66-NH₂ MOF with the adsorbed toluene were performed, quantifying the peak area at each microextraction cycle (Figure S10). In addition, the calibration process was carried out in the same experimental conditions, but with a known volume of toluene which is translated into a known toluene mass ($m_{reference}$) for a given total area (A_T) and the calibration curve was obtained.

3.4. Toluene sensing experiments

As explained in the manuscript text, the system used for the toluene sensing experiments is composed of two flow controllers: one to control the toluene flux and the other to control the nitrogen flux. These controllers allow a flux control in the 0-200 sccm (*standard cubic centimeters per minute*) range. The modification of the N₂ and the toluene/N₂ fluxes allow varying the toluene concentration in the final flux. Thus, measurements have been performed at different toluene concentrations. The toluene concentration (in parts per million-ppm) as function of the flux rate was calculated using equation (S6):

$$C = \frac{P_{tol}^* \cdot v_{tol}}{P_0 \cdot (v_{tol} + v_{N2})} \quad (S6)$$

where v_{N2} is the applied nitrogen flux (*in sccm*), v_{tol} is the applied nitrogen flux going through the saturator with the toluene (*in sccm*), P_0 the atmospheric pressure (*101 kPa*) and P_{tol}^* the vapor pressure of the toluene at room temperature (*2.886 kPa*) which is calculated using equation (S7):

$$P_{tol}^* = \exp\left(\frac{C_1}{T} + C_2 + C_3 \cdot \ln T + C_4 T + C_5 T^2\right) \quad (S7)$$

where T is the temperature and C_i are constant values ($C_1 = 80.877$, $C_2 = -6902.4$, $C_3 = -8.7761$, $C_4 = 5.8 \cdot 10^{-6}$ and $C_5 = 2$ for the toluene) [9]. A calibration curve of the toluene concentration as function of the flux in both flow controllers (v_{N2} and v_{tol}) has been developed in order to estimate the toluene concentration just by consulting this curve. In particular, the toluene

concentration (*in ppm*) as function of the toluene flux for several nitrogen fluxes (*in sccm*) is represented in Figure S12.

4. Supplementary Figures

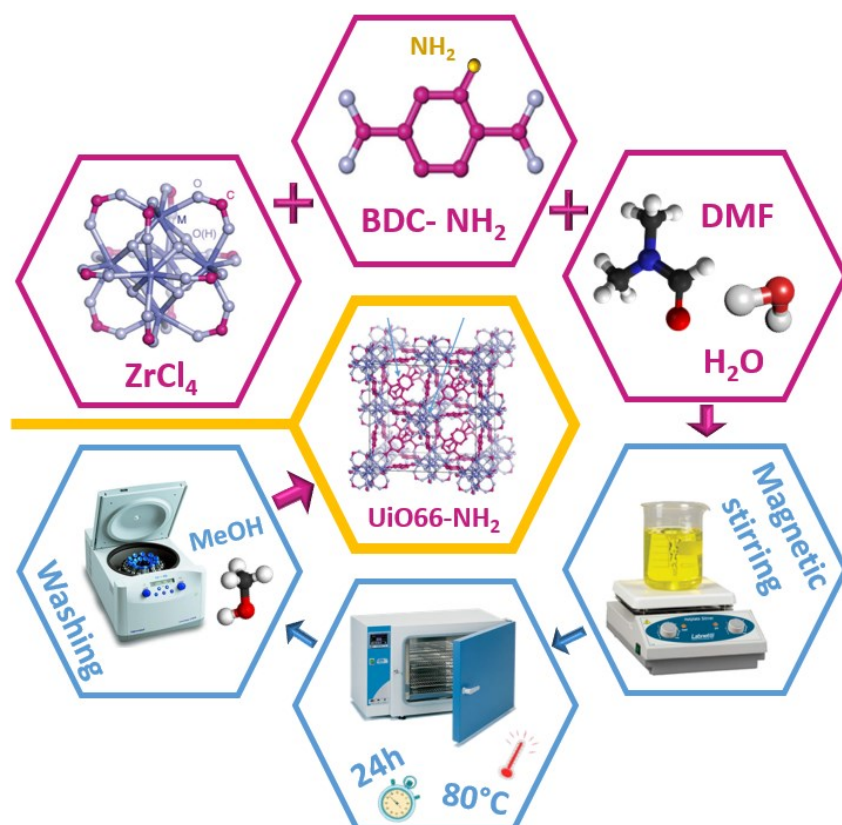


Figure S1. Schematic representation of the synthesis process of the UiO66-NH₂ MOF sample.

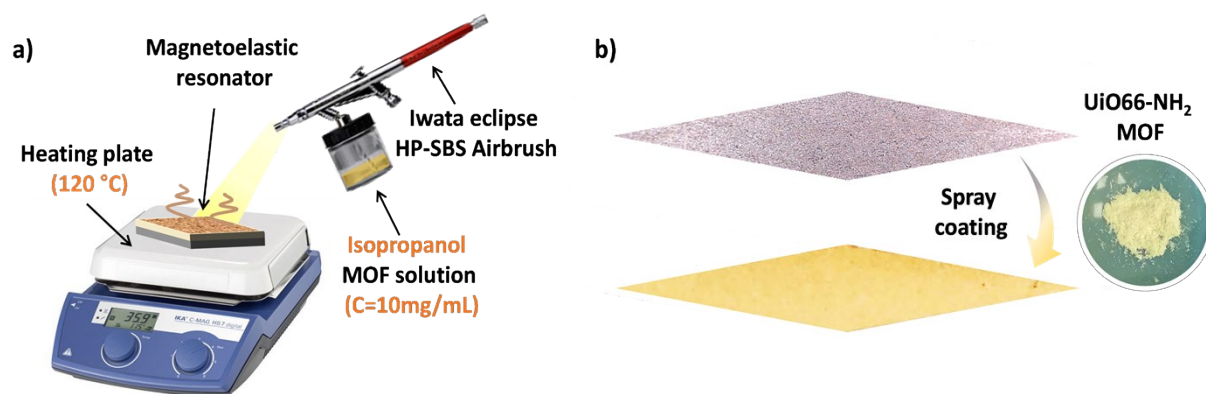


Figure S2. a) Scheme of the spray coating technique employed along this work, b) Microscope image of the magnetoelastic resonator before and after the spray coating with the UiO66-NH₂ powder MOF showed at the right.

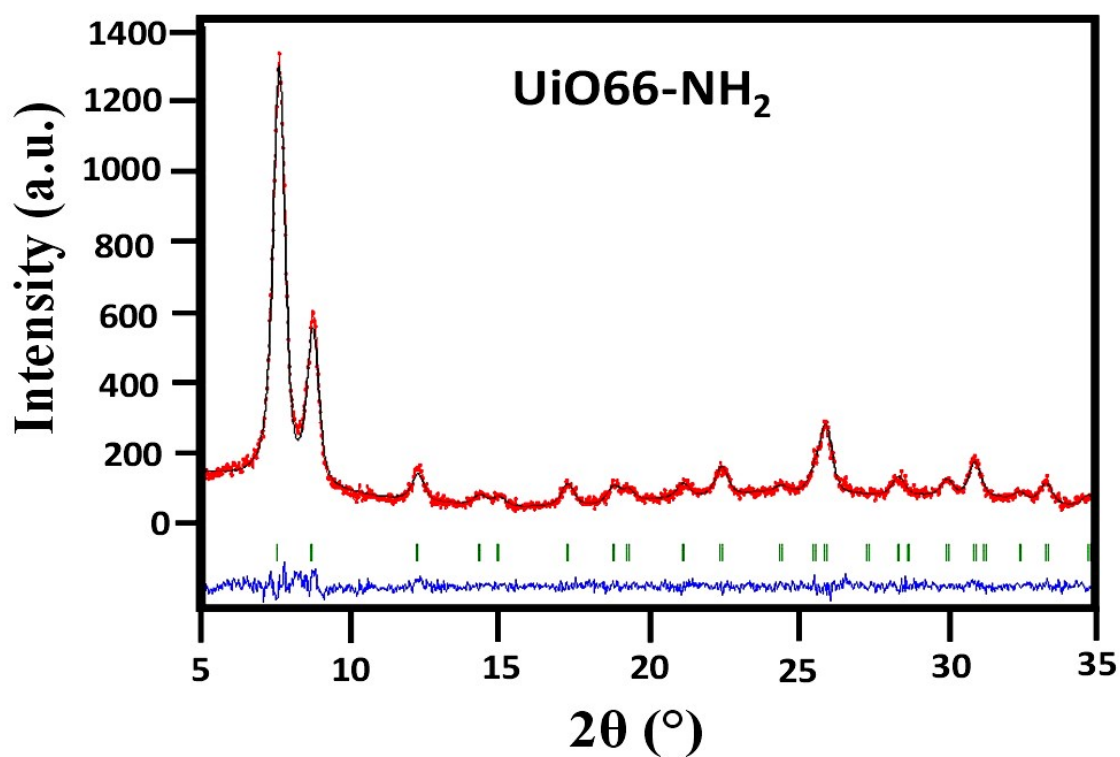


Figure S3. Powder X-ray diffraction profile matching analysis of the UiO-66-NH₂. Red points: experimental data. Black line: Calculated profile. Blue line: difference between the experimental and calculated data and (d) vertical green bars: position of the crystallographic planes.

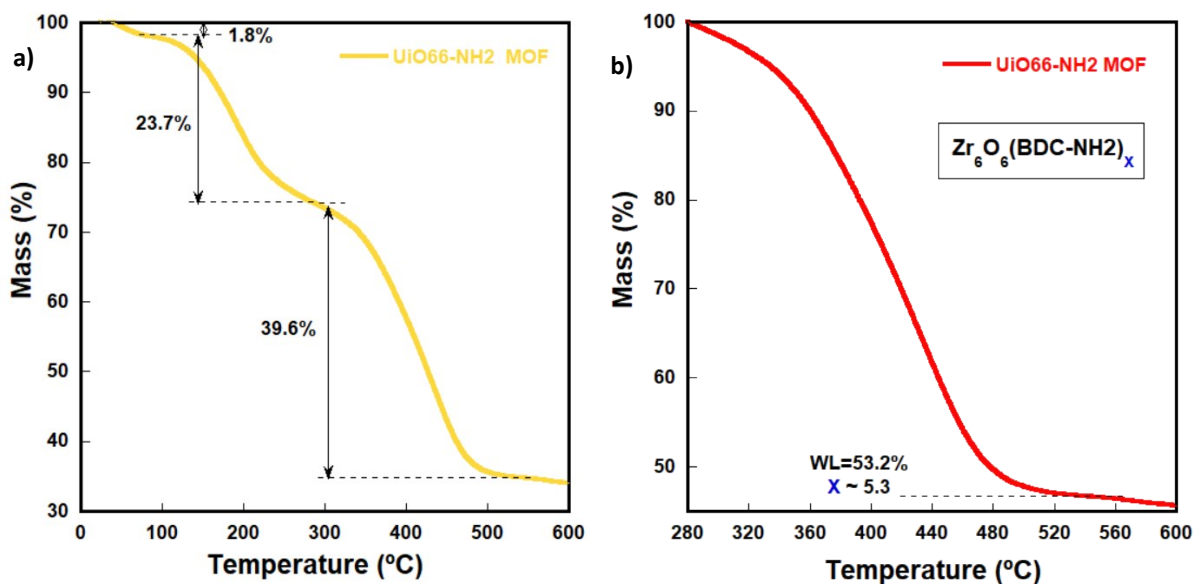


Figure S4. a) Thermogravimetric curve measured for the UiO66-NH₂ MOF. Weight loss associated to solvent release, coordinatively linked species loss (H₂O, OH and DMF) and organic linker calcination has been identified. b) Normalized TGA curve from 280 °C to 600 °C. Linker defect degree has been calculated based on the experimental weigh loss calculated from the normalized TGA curve shown in the figure (b).

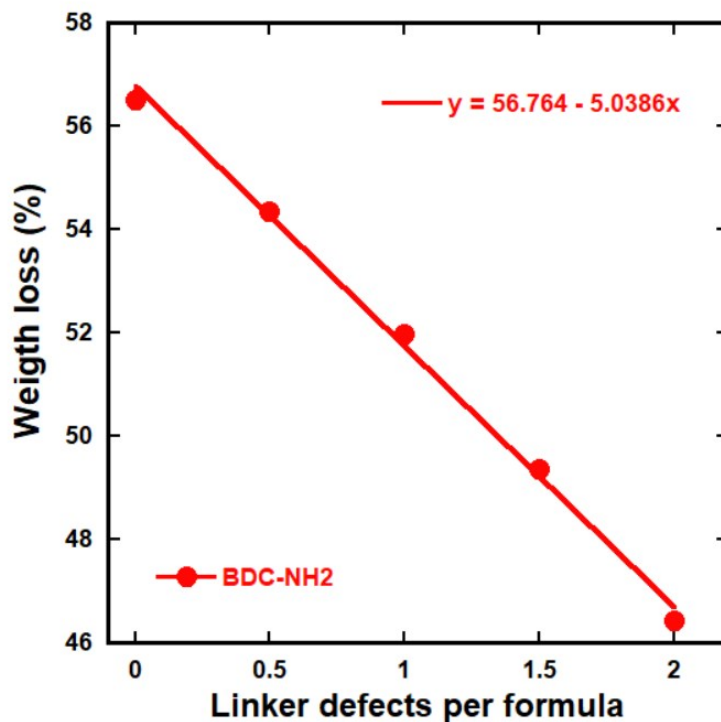


Figure S5. Theoretically calculated weight loss vs. linker defects in UiO-66-NH₂ MOF.

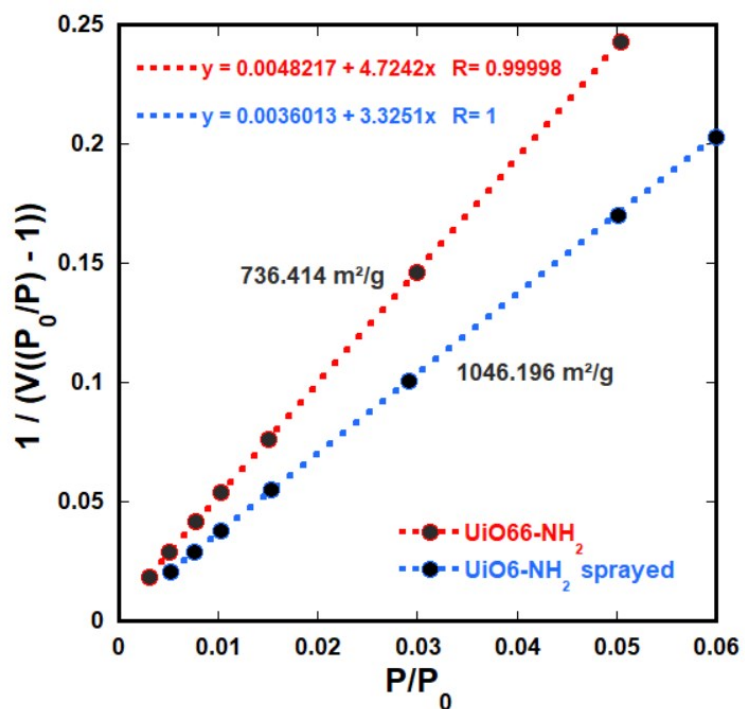


Figure S6. Fitting of the N_2 adsorption isotherms with a linearized BET model.

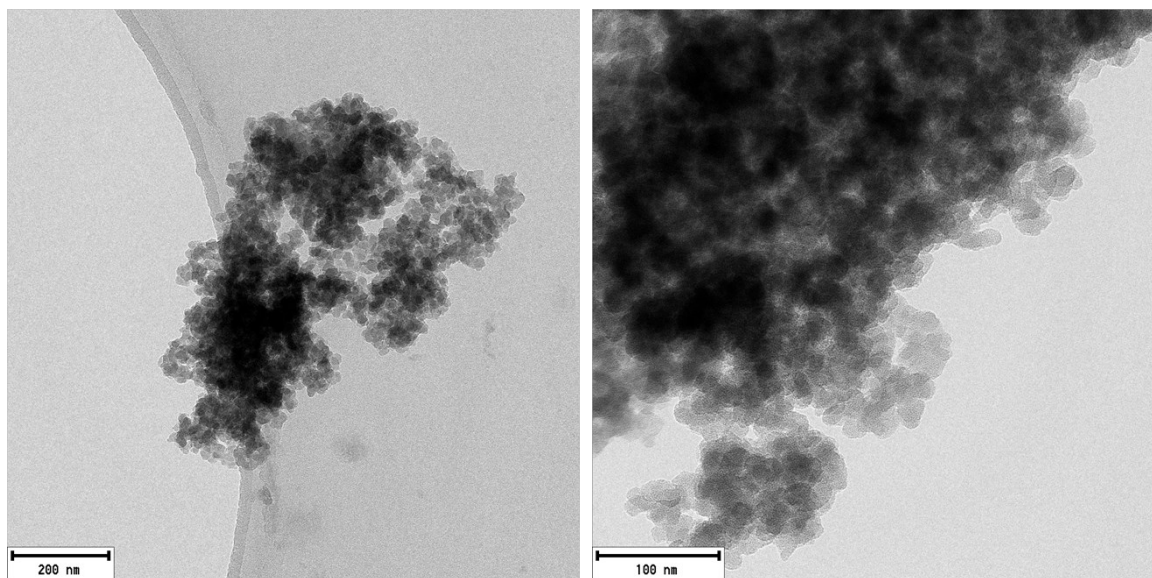


Figure S7. Transmission Electron Microscopy micrographs of the UiO-66-NH₂ sample at different magnifications.

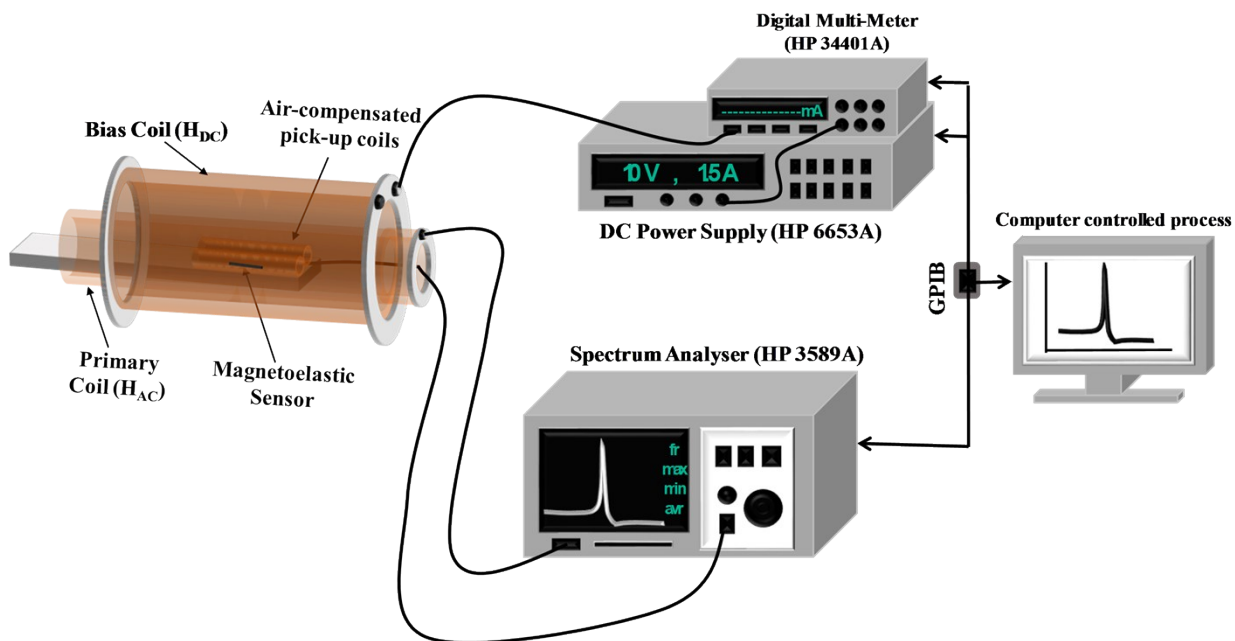


Figure S8. Scheme of the magnetoelastic set-up used for the magnetoelastic characterization.

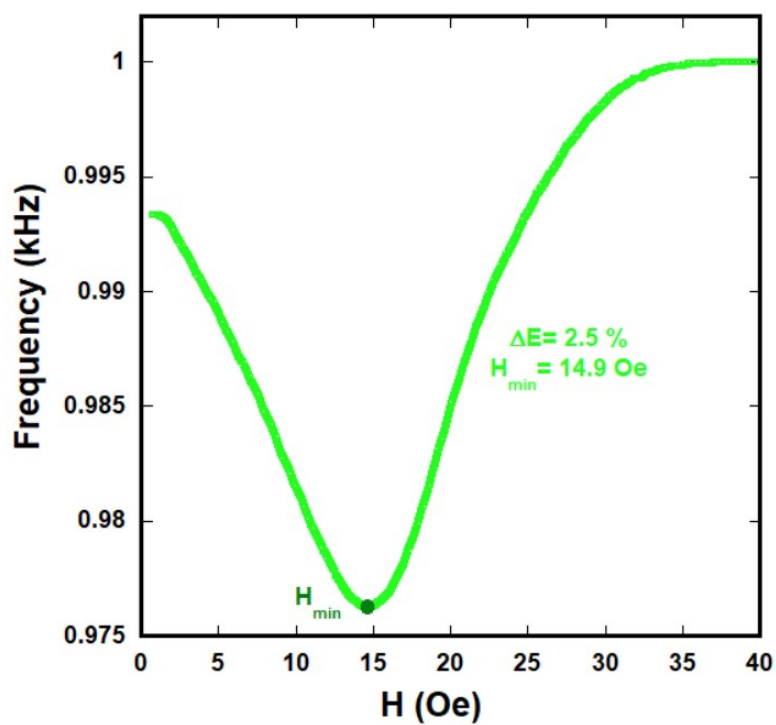


Figure S9. ΔE effect measured for the bare rhombic Metglas resonator.

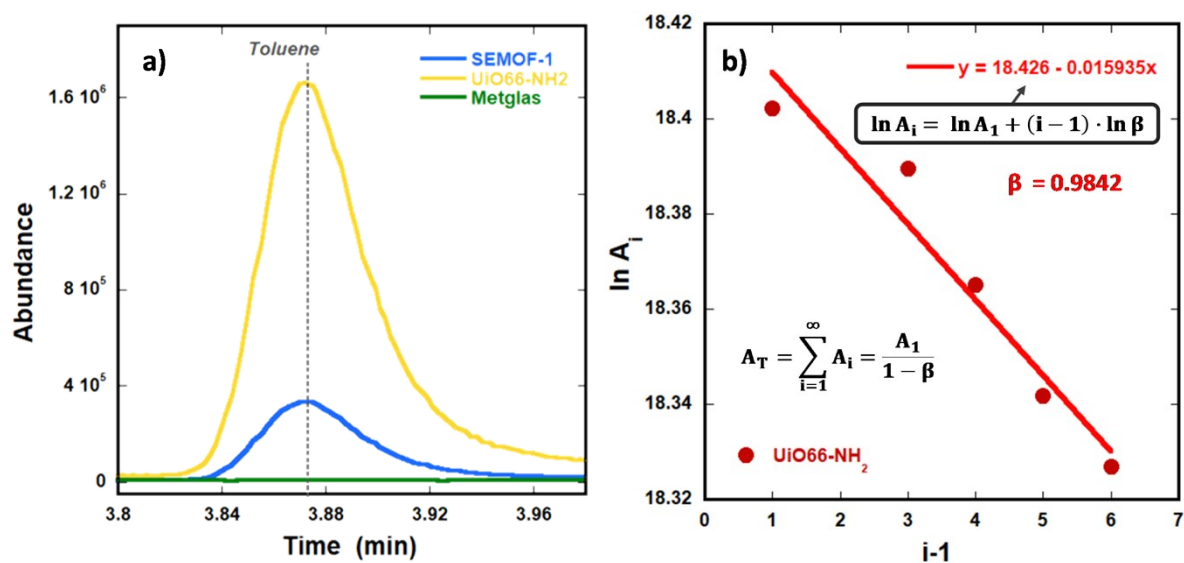


Figure S10: a) Toluene abundance measured in a bare Metglas resonator, the UiO66-NH₂ powder MOF and the UiO66-NH₂/Metglas sensor and b) UiO66-NH₂ toluene adsorption capacity calculations from the Multiple Headspace solid-phase microextractions results.

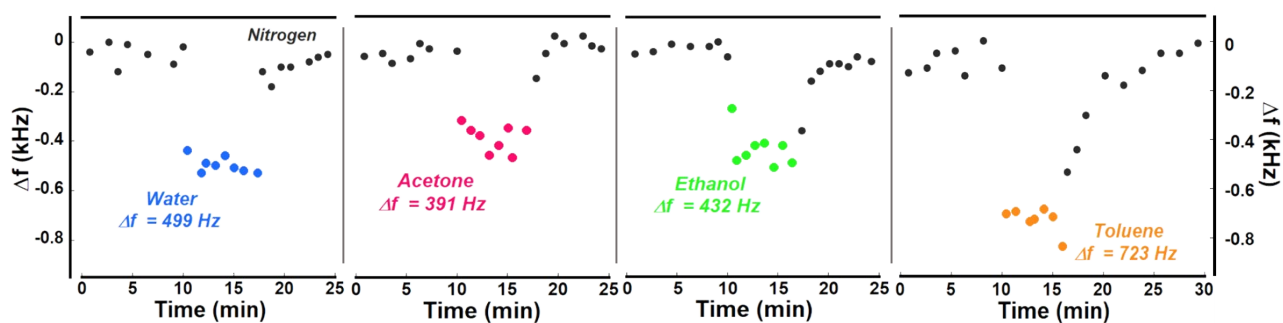


Figure S11. Selectivity experiments performed in the SEMOF-1 sensor under water, acetone, ethanol and toluene at a concentration of 8000 ppm.

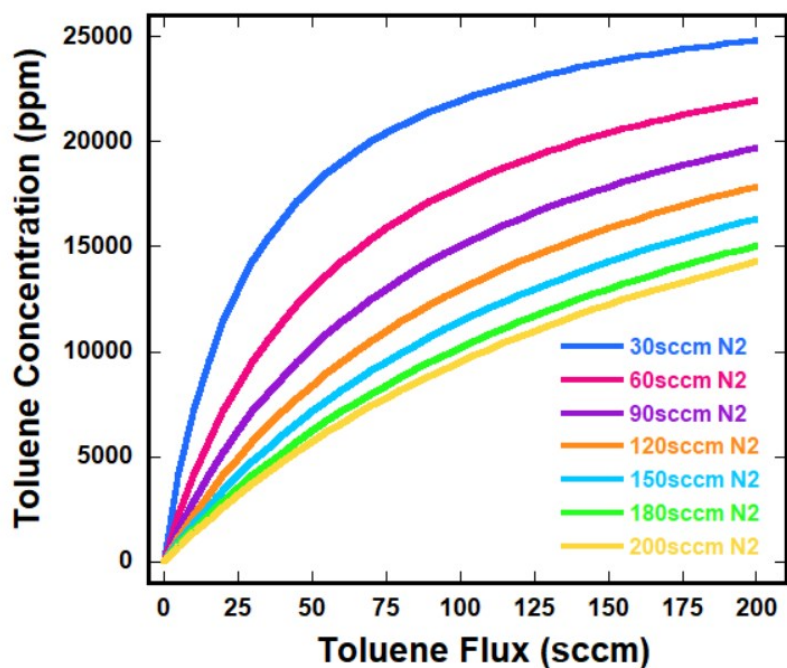


Figure S12: Toluene concentration (in ppm) as function of the toluene flux (in sccm) at different nitrogen fluxes (in sccm).

5. Supplementary Tables

Table S1. Defect degree dependence of the theoretical % weight loss due to the organic calcination in UiO-66-NH₂

Defect degree	Formula	Molecular Weight	Mw (Zr ₆ O ₁₂)	Weight Diff	% Diff
0	Zr ₆ O _{6,0} (BDC-NH ₂) _{6,0}	1699,98	739,3368	960,6432	56,5090883
0,5	Zr ₆ O _{6,5} (BDC-NH ₂) _{5,5}	1619,92	739,3368	880,5832	54,3596721
1	Zr ₆ O _{7,0} (BDC-NH ₂) _{5,0}	1539,86	739,3368	800,5232	51,986752
1,5	Zr ₆ O _{7,5} (BDC-NH ₂) _{4,5}	1459,81	739,3368	720,4732	49,3539022
2	Zr ₆ O _{8,0} (BDC-NH ₂) _{4,0}	1379,76	739,3368	640,4232	46,4155505

Table S2. Parameters obtained from the fitting of the N_2 adsorption isotherms measured for the UiO66-NH₂ and the sprayed UiO66-NH₂.

Sample	S_{BET} (m ² /g)	S_{micro} (m ² /g)	S_{ext} (m ² /g)	V_{T} (cm ³ /g)	Average half pore width (Å)
UiO66-NH ₂	736.414	645.974	90.44	1.535	7.097
UiO66-NH ₂ sprayed	1046.196	756.077	290.12	2.913	6.924

6. References

- [1] G. C. Shearer, S. Chavan, S. Bordiga, S. Svelle, U. Olsbye, and K. P. Lillerud, "Defect Engineering: Tuning the Porosity and Composition of the Metal – Organic Framework UiO-66 via Modulated Synthesis" *Chem. Mater.*, vol. 28, pp. 3749–3761, 2016.
- [2] S. Øien, D. Wragg, H. Reinsch, S. Svelle, S. Bordiga, C. Lamberti, and K. P. Lillerud, "Detailed structure analysis of atomic positions and defects in Zirconium Metal – Organic Frameworks" *Cryst. Growth Des.*, vol. 14, pp. 5370–5372, 2014.
- [3] C O. Audu, H. G. T. Nguyen, C-Y. Chang M. J. Katz L. Mao O. K. Farha, J. T. Hupp, and S. T. Nguyen, "The dual capture of AsV and AsIII by UiO-66 and analogues" *Chem. Sci.*, vol. 7, pp. 6492–6498, 2016.
- [4] S. Chavan, J. G. Vitillo, M. J. Uddin, F. Bonino, C. Lamberti, E. Groppo, K-P. Lillerud, and S. Bordiga, "Functionalization of UiO-66 metal-organic framework and highly cross-linked polystyrene with Cr(CO)₃: In situ formation, stability, and photoreactivity" *Chem. Mater.*, vol. 22, pp. 4602–4611, 2010.

- [5] K. Chul, T. Yoon, and Y. Bae, "Applicability of using CO₂ adsorption isotherms to determine BET surface areas of microporous materials" *Microporous Mesoporous Mater.*, vol. 224, pp. 294–301, 2016.
- [6] P. G. Saiz, J. Gutiérrez, M. I. Arriortua, and A. C. Lopes, "Theoretical and experimental analysis of novel rhombus shaped magnetoelastic sensors with enhanced mass sensitivity" *IEEE sensor*. (In revision stage), 2020.
- [7] B. Kolb, "Multiple headspace extraction-A procedure for eliminating the influence of the sample matrix in quantitative headspace gas chromatography" *Chromatographia*, vol. 15, no. 9, pp. 587–594, 1982.
- [8] A. A. Rincón, V. Pino, J. H. Ayala, and A. M. Afonso, "Multiple headspace solid-phase microextraction for quantifying volatile free fatty acids in cheeses" *Talanta*, vol. 129, pp. 183–190, 2014.
- [9] "Perry's Chemical Engineers Handbook", McGraw-Hill, 1999.